Article

The Importance of the Hook Region of the Cochlea for Bone-Conduction Hearing

Namkeun Kim,[1] Charles R. Steele,[2] and Sunil Puria[1,2,*]
[1]Department of Mechanical Engineering and [2]Department of Otolaryngology–Head and Neck Surgery, Stanford University, Stanford, California

ABSTRACT For the most part, the coiled shape of the cochlea has been shown to have only minor importance for air-conducted hearing. It is hypothesized, however, that this coiled shape may play a more significant role for the bone-conducted (BC) route of hearing, through inertial forces exerted by the middle ear and cochlear fluid, and that this can be tested by comparing the results of applying BC stimuli in a variety of different directions. A three-dimensional finite element model of a human middle ear coupled to the inner ear was formulated. BC excitations were simulated by applying rigid-body vibrations normal to the surface of the basilar membrane (BM) at 0.8 (d^1), 5.8 (d^2), 15.6 (d^3), and 33.1 (d^4) mm from the base of the cochlea, such that relative motions of the fluid within the cochlea produced excitations of the BM. The vibrational direction normal to the BM surface at the base of the cochlea (d^1) produced the highest BM velocity response across all tested frequencies—higher than an excitation direction normal to the BM surface at the nonbasal locations (d^2–d^4), even when the stimulus frequency matched the best frequency for each location. The basal part of the human cochlea features a well-developed hook region, co-located with the cochlear vestibule, that features the largest difference in fluid volume between the scala vestibuli (SV) and scala tympani (ST) found in the cochlea. The proximity of the hook region to the oval and round windows, combined with it having the biggest fluid-volume difference between the SV and ST, is thought to result in a maximization of the pressure difference between the SV and ST for BC stimuli normal to the BM in this region, and consequently a maximization of the resulting BM velocity.

INTRODUCTION

The cochlea is the auditory portion of the inner ear, consisting of fluid-filled chambers, the basilar membrane (BM), and the organ of Corti, which is the sensory component. The name cochlea, however, is derived from its peculiar shape. The cochlea is a spiral-shaped cavity in the bony labyrinth, which in humans makes 2.5 turns around its axis, the modiolus. The curvature of the cochlear spiral changes smoothly from the tightly curved turn at the apex to the less curved turn near the base. Due to this smooth change in curvature, the BM within the cochlear fluid chambers also exhibits smooth changes in its curvature. At the base of the cochlea, however, the curvature of the cochlear spiral and the BM changes more radically, resulting in a normal direction to the BM surface that is significantly different from those at the more-apical regions. This basal region, in which a radical change in curvature occurs, is called the hook region.

The effect of the smooth curvature of the cochlea on hearing thresholds has been studied in comparison with models representing the cochlea as a straight box shape. Viergever (1) and Steele and Zais (2) concluded, through mathematical models solving Laplace's equation, that there should be an insignificant difference in the BM velocity between a coiled BM and a straight BM in the cochlea. Contrary to their conclusions, however, others have predicted that the coiled shape should, in fact, have a significant effect on hearing, given that 1), the shear gain of the cochlear partition (defined as the ratio of shearing displacements of the tectorial membrane and the top of the organ of Corti in response to BM deflection) increases at the apex (3); and 2), the ratio of the radii of curvature from the outermost turn to the innermost turn of the cochlear spiral correlates strongly with low-frequency hearing limits (4,5). However, these studies are limited in that 1), the effect of the coiled shape on hearing was examined only for the air-conduction (AC) pathway, with the bone-conduction (BC) pathway left unconsidered; and 2), the more significant change in curvature taking place in the hook region was not considered. Recently, Steele et al. (6) modeled the full three-dimensional (3-D) behavior of the viscous fluid in the hook region of the human cochlea. Although they were able to show the evanescent wave as well as the fast wave in the scalae fluid ducts of the hook region, the effect of the hook region on BC hearing was not considered. In short, despite several studies concerning the hook region, only AC hearing, and not BC hearing, had been examined.

In BC hearing, the inertia of the middle ear (ME) ossicles and cochlear fluid are believed to play a significant role (7). Specifically, when the skull is shaken by BC inputs such as from loud sounds impinging on the head, from a tuning fork, or from a BC transducer, these inputs are thought to primarily produce an inertial input to the cochlea. Bárány (8) and Békésy (9) investigated the relationship between

Submitted July 2, 2013, and accepted for publication April 29, 2014.

*Correspondence: puria@stanford.edu

Namkeun Kim's current address is Department of Clinical and Experimental Medicine, Linköping University, Sweden

Editor: Peter Hunter.

0006-3495/14/07/0233/9 $2.00

http://dx.doi.org/10.1016/j.bpj.2014.04.052

the shaking direction of the skull and BC hearing through various measurements. Békésy posited that the human ME structure is optimized so as to minimize the hearing of one's own voice through bone conduction. He showed several characteristics of the ME ossicles that might minimize the transmission of ME inertial motions into the cochlea. For example, he showed that the skull predominantly vibrates in the vertical direction during the phonation of the vowel *oo* (as in pool), and additionally claimed that the oval shape of the stapes footplate is for the purpose of reducing the input energy into the cochlea due to such vertically oriented skull vibrations. Thus, one could expect that changing the direction of vibration could alter the rotational axes of the ME ossicles or stapes footplate, and that this could in turn affect one's sensitivity of BC hearing. Our working hypothesis is that BC vibrations presented along a direction normal to the BM surface in the hook region produce larger vibrations of the BM in comparison to BC vibrations presented in other directions. Here, it should be noted that the hook region in this study indicates the entire region over which the vestibule meets the scala vestibuli (SV), which is also where the curvature of the BM is significantly different from the more apical regions.

To test this hypothesis, we developed a 3-D finite element (FE) coiled-cochlea model of the human auditory periphery. Specifically, to investigate the effects of input direction on BC hearing, the geometry for the FE model was obtained from microcomputed tomography (μCT) images of a human-cadaver temporal bone, such that the geometry, including that of the hook region, is more anatomically realistic than that of previous models (10,11). The current model was validated by comparing model responses (e.g., the ME pressure-gain function, cochlear impedance, BM velocity, and best-frequency (BF) map) with published data (see the Supporting Material).

BC excitations were simulated by shaking the fixed bony structures of the model, such that the ME structure and cochlear fluid could experience relative vibrations depending on their coupling to the vibrating bone and their inertia. To investigate the effects of stimulation direction on BM vibration, a total of seven different shaking directions were tested and compared, consisting of 1), the x, y, and z directions of the Cartesian coordinate axes, which were respectively defined as the lateral, superior, and anterior directions of the skull; and 2), the d^1, d^2, d^3, and d^4 directions that were defined as vectors orthogonal to the BM surface at four different locations along the BM, spanning from the base to the apex. The results indicate that vibrations orthogonal to the BM at the d^1 position in the hook region dominate the response.

METHODS

Although the ME model used in this study is identical to what Homma et al. (12) and Kim et al. (10) used previously, the cochlear model is identical to the one used in another previous study (13), but without the inclusion of a superior semicircular canal dehiscence. The superior semicircular canal dehiscence was the main focus of the previous publication. The geometries of the cochlear components, including the semicircular canals, were derived from μCT scanned images of a human temporal bone. Therefore, for the current model the cochlear geometry is spiral-shaped instead of having the simplified box shape. The FE model mesh was created using HYPERMESH (Altair Engineering, Troy, MI), an FE pre/postprocessing program, and the model simulations were performed using ACTRAN (Free Field Technologies, Belgium), a vibroacoustic FE solver, which is well suited for frequency domain and vibroacoustic coupling calculations. Fig. 1 shows the current FE model of the human auditory periphery, consisting of the ME and cochlea, and including the semicircular canals. A detailed description of the ME structure can be found in Homma et al. (12).

Due to the spiral cochlear geometry, the mechanical properties of some components (i.e., the BM, stapes annular ligament, and round window (RW)) were tuned to make the model results consistent with published experimental data (see the Supporting Material) such as a map of the BF locations along the BM (14), as well as ME transfer functions (15–18).

Material properties

Material properties for the FE model were reported previously (10), except for the RW, stapes annular ligament, and BM, because the properties of those components were altered from the previous model due to the modified geometry. The density of the RW membrane was set to 1200 kg/m^3, its Young's modulus was set to 0.05 MPa, and its loss factor was set to a frequency-independent value of 0.8. The density of the stapes annular ligament was also set to 1200 kg/m^3, but its Young's modulus was set to 0.7 MPa, and its loss factor was set to vary linearly with the log-scaled frequency, such that its value was 0.017 at 0.1 kHz, 0.17 at 1 kHz, and 1.7 at 10 kHz. In this study, the BM was divided into 35 sections of equal length. To model the stiffness change along the length of the BM, the Young's modulus of the BM was gradually decreased from the base to the apex (i.e., from 6.5 to 5.5 MPa in the longitudinal direction, and 0.2

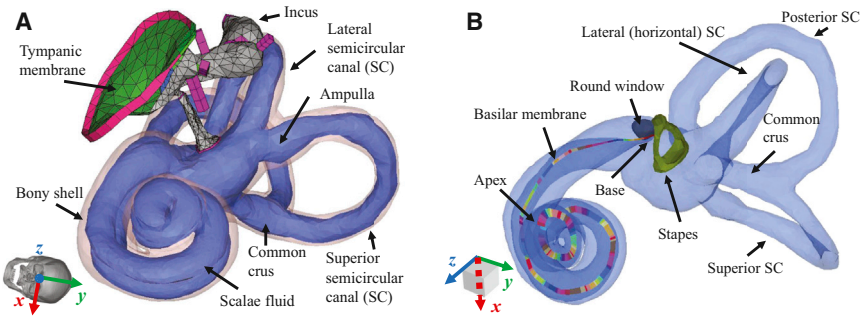

FIGURE 1 An FE model of the human auditory periphery. (*A*) ME structures, the bony shell of the cochlea (*light pink*), and the scalae fluid (*light purple*), including the semicircular canals. (*B*) The stapes, RW, and BM. The SV is connected to the ST through the helicotrema, which is a hole located at the end of the BM at the apex. The various colors along the BM are used solely to distinguish neighboring sections, with each section having its own Young's modulus and set of local coordinates. The global x, y, and z directions correspond to the lateral, superior, and anterior directions of the skull, as shown by the tilted skull image of panel *A*. To see this figure in color, go online.

to 0.1 GPa in the transverse direction, with a loss factor of 0.3). The density of the BM was assumed to be 1000 kg/m^3, because the density of soft tissue is usually assumed to match that of water, and its orthotropic material properties were determined by tuning the Young's moduli to make the BF-to-place cochlear map reasonably consistent with experimental data (14). The orthotropic ratio (E_x/E_y, where E_x and E_y are the Young's moduli for the local longitudinal and transverse directions relative to the BM, respectively) was nearly 0.03 throughout. The detailed process for tuning the model has been described previously (10). It should be noted that the fluid in both the SV and ST is assumed to be almost incompressible, because the speed of sound in fluid is a high but finite (i.e., not infinite) value of 1500 m/s.

The model geometry and FE mesh

The BM width changed linearly from 170 μm at the base to 500 μm at the apex, and the thickness changed from 7 μm at the base to 0.9 μm at the apex. The BM was meshed using 18,400 six-noded pentahedral shell elements, and the RW was meshed using 400 four-noded tetrahedral elements. The SV and ST cochlear fluid chambers were meshed using 518,600 four-noded linear tetrahedral elements.

With the inclusion of the semicircular canals in the current model, their ~120 mm^3 of additional fluid volume brought the total fluid volume to 280 mm^3. The fluid in the cochlea was all assumed to be perilymph, so the scala media containing the endolymph fluid has been collapsed into the cochlear partition, whose properties are dominated by the pectinate zone of the BM. In addition, the present model formulation is for passive mechanics and does not consider the active cochlear amplification mechanisms (19–22).

Simulations using AC or BC excitation

AC excitation was simulated by assigning a uniformly distributed dynamic unit pressure over the tympanic membrane surface on the ear canal side. Fixed-displacement boundary conditions were applied to boundaries of the structure, such as the ends of the ligaments and tendons, the edge of the tympanic annulus, and the bony shell of the cochlea. On the other hand, among the inertial and compressional inputs to the cochlea thought to be important for BC hearing (23), only the inertial component is considered here. The inertial BC excitations were simulated by assigning sinusoidal displacement vectors of equal magnitude and direction at the boundaries of the model. These boundaries include the wall of the cochlea and the ends of the ME supporting structures such as the incus ligament, tensor tympani muscle, anterior ligament, lateral ligament, stapedius tendon, and tympanic annulus. Assigning directional vibrations to these boundary conditions effectively produces rigid body vibrations of the bony parts of the temporal bone. It should be noted that in reality, the strain of the bone may not be negligible at high frequencies, such that the outer bony shell may not move in-phase with one another. However, in this simulation, because the bone was assumed to have a high Young's modulus, the outer bony shells do show in-phase movement within the simulated frequency range. The directions of excitation corresponded to the x, y, and z axes defined in Fig. 1, which represent the lateral, superior, and medial directions of the skull, respectively; and to vectors normal to the BM surface at four locations between the cochlear base and apex, i.e., d^1–d^4, as defined in Fig. 2. The magnitude of the applied displacement vector, D_b, was 0.01 μm for each of these directional vibrations. Although this magnitude was selected arbitrarily, it was large enough to reveal the inertial effects of the ME ossicles and fluid in the cochlea. Because this is a linear model, the cochlear responses were not affected by the choice of input magnitude, since the output variables were normalized by the relevant input variable, such as the input velocity or input volume velocity into the cochlea.

The d^1, d^2, d^3, and d^4 directions shown in Fig. 2 constitute directions normal to the BM surface at distances from the base of the cochlea of, respectively, 0.80, 5.80, 15.63, and 33.06 mm. Although d^1–d^4 were all defined to be normal to the local BM surface, the coiled and angled shape of the BM is such that the orthogonal vector components of these four directions were different enough from one another so as to stimulate different 3-D motions of the BM. These BC simulations with different excitation directions were performed both with and without the ME ossicles, to distinguish the inertial contributions of the ME ossicles from those of the cochlear fluid by itself. Removing the ME ossicles was implemented by deleting all of the ME components except for the stapes and stapes annular ligament, and then essentially removing any remaining inertial contribution from the stapes by decreasing its density by two orders of magnitude.

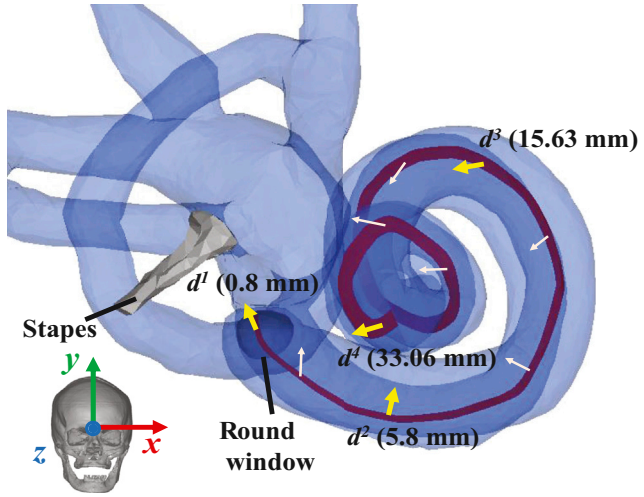

FIGURE 2 Directional vectors of simulated BC stimuli, denoted by x, y, z, d^1, d^2, d^3, and d^4. As in Fig. 1, the x, y, and z directions correspond to the lateral, superior, and anterior directions of the skull (see *inset image*), respectively. The thick yellow arrows, for d^1, d^2, d^3, and d^4, represent stimuli normal to the BM at distances 0.8, 5.8, 15.63, and 33.06 mm from the base, respectively. The thin light-pink arrows represent normal directions to the BM at intermediate positions. To see this figure in color, go online.

Decomposition analysis for pressures in the scalae fluid, and BM velocity

The SV and ST fluid pressures along the BM length, $P_{SV}(\chi)$ and $P_{ST}(\chi)$, respectively, were calculated for model elements directly adjacent to the BM surface, on the longitudinal centerline of the BM. $P_{SV}(\chi)$ and $P_{ST}(\chi)$, and the volume velocities of the oval window (U_{OW}) and round window (U_{RW}), were decomposed into symmetric components, $P_S(\chi)$ and U_S, and antisymmetric components, $P_A(\chi)$ and U_A, according to the following equations (10):

$$\begin{aligned} P_S(\chi) &= \frac{1}{\sqrt{2}}[P_{SV}(\chi) + P_{ST}(\chi)], \\ U_S &= \frac{1}{\sqrt{2}}[U_{OW} + U_{RW}], \\ P_A(\chi) &= \frac{1}{\sqrt{2}}[P_{SV}(\chi) - P_{ST}(\chi)], \ \textit{and} \\ U_A &= \frac{1}{\sqrt{2}}[U_{OW} - U_{RW}]. \end{aligned} \tag{1}$$

The BM velocity along the BM length, $V_{BM}(\chi)$, was calculated in the direction normal to the BM surface at each of the locations, χ.

Validation of the FE model, and cochlear responses to AC and BC excitation

The responses of the current model (e.g., the ME pressure-gain function, cochlear impedance, BM velocity, and BF map) were compared against published data (see the Supporting Material). In addition, the cochlear responses to AC and BC excitation were calculated to verify their consistency with the previous model's (10) cochlear responses (not shown). The detailed processes of model validation are described in the Supporting Material.

RESULTS

Directional effects of BC excitation

Varying the vibratory direction for a fixed input frequency

The BC excitations were simulated in the x, y, z, d^1, d^2, d^3, and d^4 directions (see Fig. 2). The resulting relative BM velocities for these excitation directions are respectively denoted as V^x, V^y, V^z, V^{d1}, V^{d2}, V^{d3}, and V^{d4}; and each of these was normalized by the BM velocity for the d^1 directional excitation (V^{d1}) to reveal any differences due to the direction of the BC excitation. Note that in taking these ratios, both velocities are, in fact, relative BM velocities of the form $\Delta V_{BM} = V_{BM} - V_B$, where V_{BM} is the BM velocity and V_B is the velocity of the bone, even though we drop the preceding Δ and the subscript BM from the notation for convenience and refer to them simply as velocity ratios (e.g., V^{d1} is defined as $V_{BM}{}^{d1} - V_B{}^{d1}$, where $V_B{}^{d1}$ is the BC velocity in the d^1 direction used to stimulate the model). If the velocity ratios between each case and the d^1 directional excitation (V/V^{d1}) are below 0 dB for every simulated frequency, then the BM-velocity magnitudes for the d^1 directional excitation (V^{d1}) are higher than those for the other directional excitations (V^{d2}, V^{d3}, and V^{d4}). Figs. 3 and 4 present these normalized BM velocities, of the form V/V^{d1}, up to the BF positions at 0.5 kHz (24 mm; *A*), 1 kHz (20 mm; *B*), and 7 kHz (8 mm; *C*), both without (Fig. 3) and with (Fig. 4) the ossicular inertia of the middle ear. As can be seen in Figs. 3 and 4, the magnitude of every normalized result lies below 0 dB, except for the case of V^x/V^{d1} with the middle ear at 1 kHz, which means that the magnitude of the BM velocity due to the d^1 directional excitation is almost always higher than those due to the other directional excitations. Interestingly, although the V^y/V^{d1} ratios were decreased by ~2 dB after adding the ME ossicles, the ratios for the other directions were all increased due to the added ME inertia. However, because each velocity in the plotted ratios is affected differently by the presence or absence of the ME inertia, according to the excitation direction, it is difficult to determine the specific effects of the ME inertia for a given excitation direction based on the ratios shown in Figs. 3 and 4 alone. For this reason, see Fig. 7, which plots velocity ratios for each excitation direction between the case without the ME and the case with the ME, thus allowing the effects of the ME for each excitation direction to be seen directly.

Varying the input frequency for a fixed vibratory direction

Figs. 5 and 6 are based on the same kind of BM velocity distribution results shown in Figs. 3 and 4, plotted up to the BF position and normalized by the velocity of the d^1 directional excitation (V/V^{d1}), except each panel now corresponds to just one excitation direction and contains curves for a total of 24 different stimulus frequencies (spaced every 0.1 kHz from 0.5 to 1 kHz, and every 0.5 kHz from 1 to 10 kHz), without the ME structure (Fig. 5) and with the ME structure (Fig. 6). Because every line is shown up to the BF position corresponding to the input frequency, the lines feature different lengths along the horizontal axis of the figures. The frequency is indicated by the coloring of the lines, with blue-violet representing 0.5 kHz, and red-brown representing 10 kHz.

In summary, in Figs. 3–6, all of the simulated velocity ratios (relative to V^{d1}) are <0 dB, except for V^x with the ME structure at 1 kHz, showing that the d^1 velocity almost always produces the largest simulated BM magnitude.

Fig. 7 shows the relative BM velocity without the ME mass ($V^{no\ ME}$) normalized by the relative BM velocity with the ME mass (V^{ME}), for each vibrational direction (x, y, z, d^1, d^2, d^3, and d^4). The lines for all directions in Fig. 7 reach their lowest values near 1.5 kHz, and most values of the ratios lie below 0 dB, which indicates that the velocities tend to be smaller in the absence of the ME ossicles contributing their inertia. Exceptions to this, in which the velocities become larger without the presence of the ME ossicles, include the values for the y, z, and d^1 directions below 1 kHz and above 5 kHz, and the values for the x and d^4 directions below 0.6 kHz.

DISCUSSION

Directional effects

Effects of the d^1 directional excitation of the hook region

Figs. 3 and 4 show the BM velocity distributions along the length of the BM for six different directions of BC stimulation (x, y, z, d^2, d^3, and d^4) and for three different input frequencies (0.5, 1, and 7 kHz), with each result normalized by the BM velocity due to the d^1 directional BC excitation. All of the calculated BM velocity ratios have a magnitude of <0 dB, with the sole exception of the x-directional BC excitation with the ME structure at 1 kHz (see Fig. 4 *B*), which means that the BM velocity due to the d^1-directional BC stimulation (V^{d1}) has a larger magnitude than the BM responses for all the other directional BC inputs. Furthermore, Figs. 5 and 6 show that V^{d1} has the largest magnitude among all the simulated frequencies from 0.5 to 10 kHz, for the given BC excitations in the d^2, d^3, and d^4 directions. Even compared to when the direction of the BC input is normal to the BF location on the BM corresponding to the input frequency, the d^1 direction still ends up having a

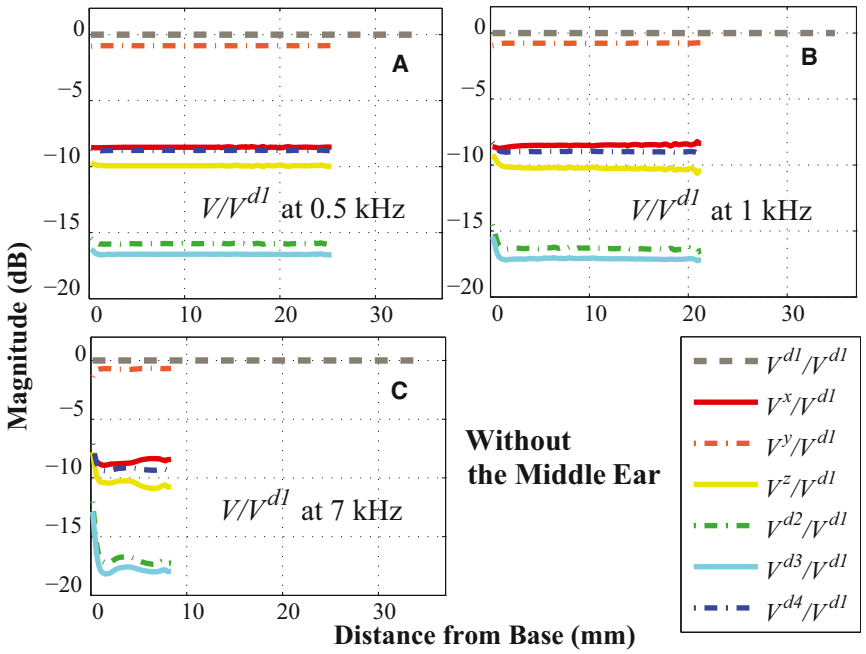

FIGURE 3 (*A–C*) Ratios of the BM velocities, V/V^{d1}, for BC excitations at (*A*) 0.5 kHz, (*B*) 1 kHz, and (*C*) 7 kHz. Every *V* represents a relative BM velocity, $\Delta V_{BM} = V_{BM} - V_B$, for a given excitation direction. For this figure, the ME structure was not included. To see this figure in color, go online.

more significant effect on the BM response. For example, consider a 3 kHz input frequency, whose BF position on the BM is ~15 *mm* from the base (see Fig. S4 in the Supporting Material). In this study, the d^3 direction is normal to the BM at 15.63 mm from the base, which is close to the BF position for a 3 kHz input frequency; but even though the d^3 direction is normal to this BF position, Figs. 5 *B* and 6 *B* show that the d^1-directional excitation for 3 kHz still generates a higher BM velocity than the d^3-directional excitation.

Based on this observation, it can be said that the inertial effects of BC excitation can differ depending on the direction of the excitation. It appears that the vibratory direction normal to the BM in the hook region of the cochlea affects the BM velocity most significantly, thus providing computational evidence to support our hypothesis that the normal directional vibration to the BM surface at the cochlear base would produce the maximum BM velocity. The precise mechanism for this is not well understood. However, one anatomical observation is that the difference in the

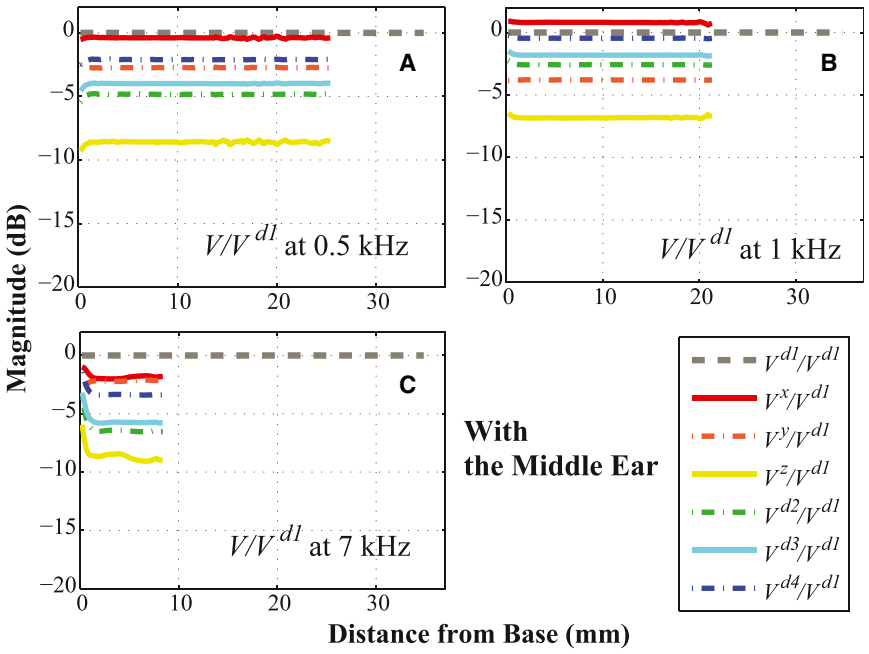

FIGURE 4 The same as Fig. 3, except the ME structure was included. To see this figure in color, go online.

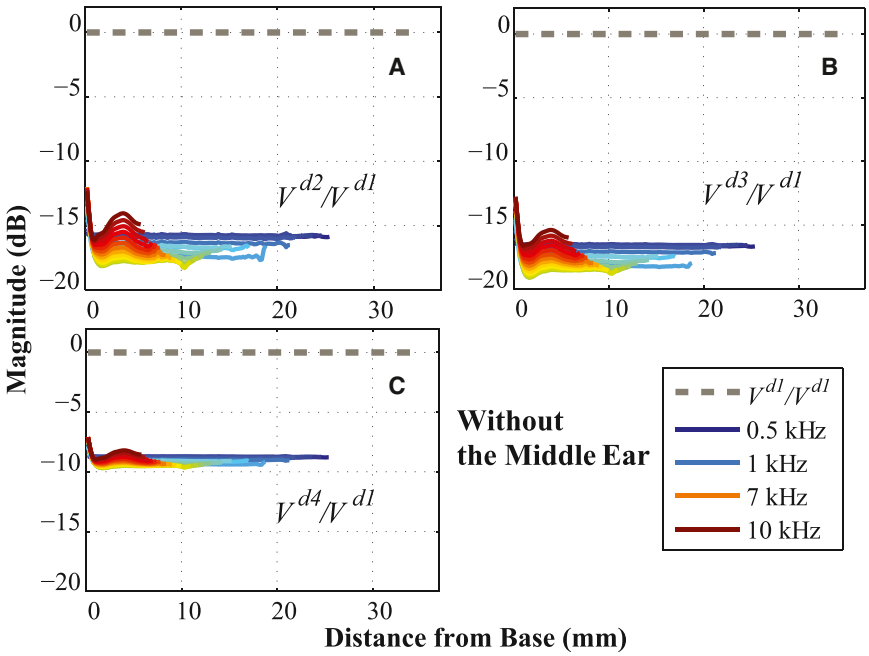

FIGURE 5 Ratios of BM velocities for different excitation directions, (*A*) V^{d2}/V^{d1}, (*B*) V^{d3}/V^{d1}, and (*C*) V^{d4}/V^{d1}, for 24 frequencies from 0.5 to 10 kHz (spaced every 0.1 kHz from 0.5 to 1 kHz, and every 0.5 kHz from 1 to 10 kHz). As in Figs. 3 and 4, every V represents a relative BM velocity, $\Delta V_{BM} = V_{BM} - V_B$, for a given excitation direction. In the legend, only four frequencies (0.5, 1, 7, and 10 kHz) among all the simulated frequencies are marked. For this figure, the ME structure was not included. To see this figure in color, go online.

cross-sectional areas of the SV and ST happens to be largest in the vicinity of the hook region at the base of the cochlea. We hypothesize that this large difference in cross-sectional areas between the SV and ST in the hook region can cause a more significant antisymmetric pressure component to emerge in the SV and ST across the BM when the direction of the BC excitation is normal to the BM surface in this region. Fig. 8 shows the ratios of the antisymmetric component of the scalae fluid pressure of the six directions (x, y, z, d^2, d^3, and d^4) relative to the d^1 direction, $P_A/P_A{}^{d1}$, which are calculated at the BF position for each input frequency. Fig. 8 indicates that BC excitation in the d^1 direction almost always produces the largest P_A magnitude, because the ratios are all <1 except for the x direction between 0.8 kHz and 1.3 kHz. Future calculations that involve systematic changes to the cochlear geometry in the vestibule region are needed to come to conclusions about this hypothesis. The exceptional case, the x-directional vibration, will be discussed in the next section.

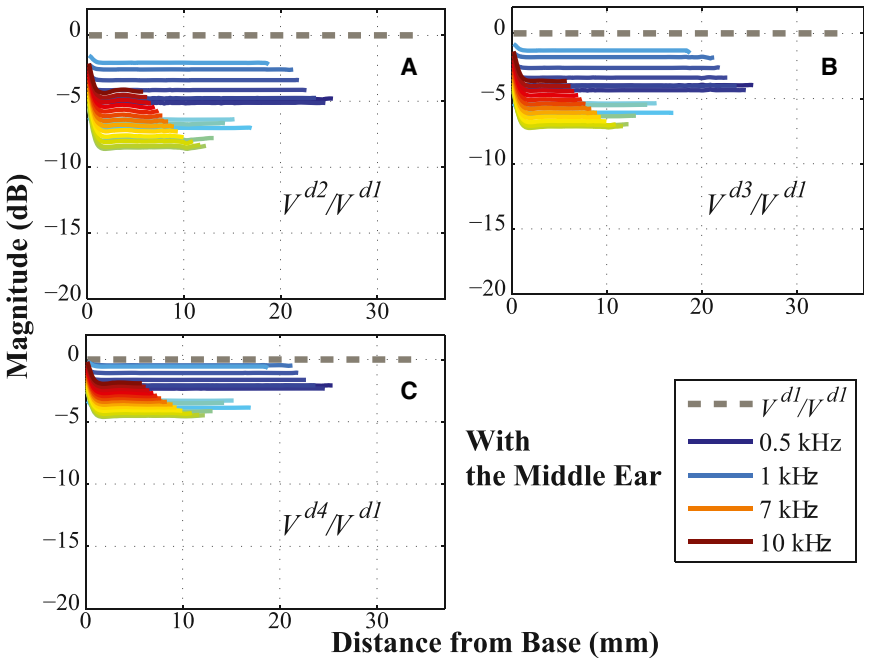

FIGURE 6 The same as Fig. 5, but with the ME structure included. To see this figure in color, go online.

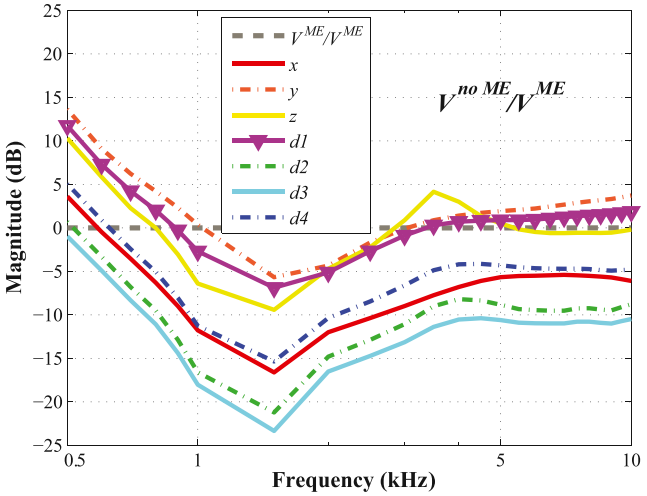

FIGURE 7 Ratios of the relative BM velocity in each vibrational direction (i.e., x, y, z, d^1, d^2, d^3, and d^4), between cases without the ME ($V^{no\ ME}$) and with the ME (V^{ME}). To see this figure in color, go online.

Effects of the directional excitation of the ME

Fig. 7 shows that the values of V^y at 1 kHz are the same with or without the ME (i.e., the ratio is ~0 dB), whereas at the same frequency V^z with the ME is ~6 dB larger than without the ME and V^x with the ME is ~12 dB larger than without the ME. This unusually high contribution of the ME inertia to the BM velocity under x-directional stimulation can be said to contribute to the exceptional case of the response due to the x direction exceeding that due to the d^1 direction at 1 kHz, as shown in Fig. 4 *B*. Based on these observations, it could be expected that the ME ossicles would contribute to BC hearing by differing amounts depending on the excitation direction. In addition, comparing the results of Figs. 3 and 4 supports the idea that the direction of excitation affects how much the ME ossicles contribute to BC hearing. For example, when there are no ME ossicles (Fig. 3), V^{d3} shows the lowest values relative to V^{d1} among all six results. However, when the ME ossicles are added (Fig. 4), V^{d3} rises to third or fourth place among the six different results. Due to the direction-dependent effects of the ME ossicles, the relative ordering of the BM-velocity magnitudes among different directional results can change depending on whether the ME is present or not. Bárány (8) already predicted such direction-dependent effects of the middle ear. Stenfelt et al. (24) found that different directions of vibration (orthogonal to one another) caused differences in magnitude of at most 5 and 12 dB for the stapes footplate and umbo velocities, respectively. Fig. 9, *A* and *B*, plot the stapes footplate and umbo velocities resulting from each directional excitation. The stapes footplate velocities are presented as $\Delta V_{\mathrm{STAPES}} / V_{\mathrm{B}}$, where $\Delta V_{\mathrm{STAPES}} = V_{\mathrm{STAPES}} - V_{\mathrm{B}}$, V_{STAPES} is the stapes footplate velocity, and V_{B} is the bone velocity; and the umbo velocities are presented in an analogous way, as $\Delta V_{\mathrm{UMBO}} / V_{\mathrm{B}}$. The magnitudes of the velocity vectors for the stapes footplate and umbo were calculated as projections onto the normal direction of the stapes footplate and umbo, respectively. In Fig. 9 *A*, although the differences in the stapes footplate velocity between two orthogonal directions, x and y, are within 5 dB, the z-directional results show a difference of ~5–10 dB. Similarly, in Fig. 9 *B*, the z-directional results show a difference of ~10–20 dB or more when compared with the y-directional results. Additionally, the different levels of the stapes footplate and umbo velocities in Fig. 9 provide further evidence of the existence of direction-dependent effects of the ME in response to BC stimuli. In this simulation, because the stapes footplate contacts the fluid in the SV, the stapes footplate and umbo velocities are affected by the fluid inertia as well as the ME inertia. Therefore, care must be taken when attempting to draw conclusions about which direction drives the maximum ME inertia. However, based on the higher stapes footplate and umbo velocities in Fig. 9, *A* and *B*, it appears that the d^1 direction can produce significant effects in the ME inertia as well as in the cochlear fluid inertia.

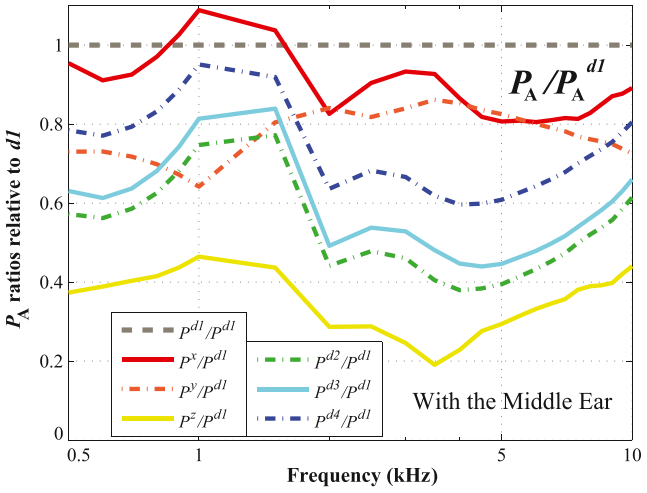

FIGURE 8 Ratios of the antisymmetric scalae fluid pressure components, P_A/P_A^{d1}, for all six directions (i.e., x, y, z, d^2, d^3, and d^4), calculated at the BF position for each input frequency. To see this figure in color, go online.

The relative effects of excitation direction on cochlear fluid inertia versus ME inertia

In comparing cases without and with the ME, three points should be discussed. First of all, the addition of the ME mass generally served to increase the BM velocity, which corresponds in Fig. 7 to the ratios of the absolute BM velocities being below 0 dB. Specifically, in the 1–2 kHz range, the effects of the ME mass on the BM velocity were the most significant (up to 24 dB). The 1–2 kHz range is well known to be where the resonance frequency of the ME exists for BC excitation (25,26). Therefore, the Carhart's notch

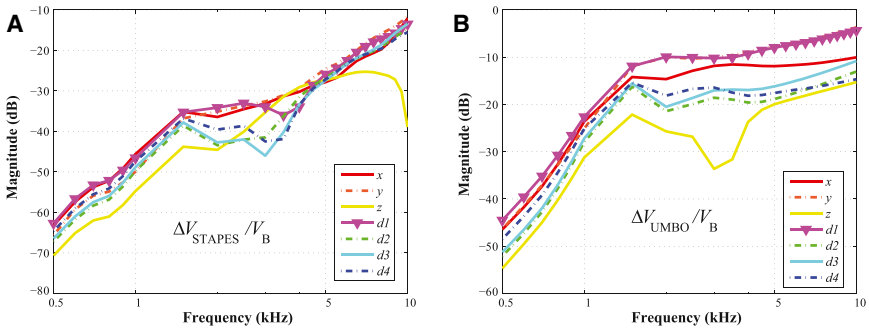

FIGURE 9 (*A*) Stapes footplate and (*B*) umbo velocities in response to BC excitation for each vibrational direction (i.e., *x*, *y*, *z*, d^1, d^2, d^3, and d^4). The stapes footplate velocity is presented as $\Delta V_{STAPES} / V_B$, where $\Delta V_{STAPES} = V_{STAPES} - V_B$, V_{STAPES} is the stapes footplate velocity, and V_B is the bone velocity; and the umbo velocity, $\Delta V_{UMBO} / V_B$, is presented in an analogous way. The magnitudes of the velocity vectors for the stapes footplate and umbo were calculated as projections onto the normal direction of the stapes footplate and umbo, respectively. To see this figure in color, go online.

phenomenon (25), which involves a dip in the BC audiogram around 2 kHz as a result of otosclerosis, could be explained by the loss of ME inertial motion due to ossification of the stapes annular ligament.

The second point has to do with the case in which the ME ossicles are not included, such that the effects of the inertia of the cochlear fluid are all that is shown. The *y* direction (i.e., the superior direction relative to the skull) happens to have the smallest angle difference with respect to the d^1 direction (33°, versus 60°–80° for the other directions, which are d^2, d^3, d^4, *x*, and *z*), and as a consequence of this, the antisymmetric pressure component (and resulting BM velocity ratio) ends up being higher for the *y* direction than for the other directions, except d^1. Therefore, V^y/V^{d1} is the closest to V^{d1}/V^{d1} in Fig. 3. This similar behavior between the d^1 and *y* directions, as compared to the other directions, is easiest to observe when the ME ossicles are not present, because the inclusion of the ME affects V^{d1} somewhat differently than V^y (Fig. 7).

Finally, in Fig. 7, the closer a line is to the flat reference line, the less significant the added ME inertia is to the BM velocity. The results for the d^1 and *y* directions tend to be the closest to this reference line, so the BM velocities for these directions are therefore affected less by the presence of the ME than is the case for the other directions. This can be explained by the relatively large effects of the cochlear fluid inertia for excitations in the d^1 or *y* directions (Fig. 3), such that the addition of the effects due to ME inertia has a relatively small influence on the total for these directions. One could consider, on the other hand, that proximity to the reference line in Fig. 7 could have more to do with a relatively smaller effect from the ME inertia rather than a relatively larger effect from the cochlear fluid. However, in Fig. 9 *A*, the stapes footplate velocities for the d^1 and *y* directions are either the highest or within only a few dB of being the highest, which suggests that the effects of the ME inertia are relatively large for those directions. On the other hand, for the *z* direction, the relatively low stapes velocity values in Fig. 9 *A* suggest that the proximity to the reference line in Fig. 7 has more to do with the ME inertia having a relatively small effect in that direction.

CONCLUSION

FE model simulations of the human auditory periphery, consisting of both the ME and the cochlea, were performed to gain insight into the mechanics of BC hearing. The geometry of the ME and the coiled cochlea, including the semicircular canals, was obtained via μCT imaging. The model results for both AC and BC stimuli are consistent with previous modeling studies (10) in that regardless of excitation type or direction, the antisymmetric fluid pressure is highly correlated with the BM velocity (see the Supporting Material). Detailed analyses using this model indicate that the directional BC vibrations normal to the BM in the basal hook region of the cochlea affect the BM responses most significantly when compared to other directions of BC excitation. It is hypothesized that, due to the asymmetric cross-sectional areas of the SV and ST in the hook region, the directional BC vibrations normal to the BM in that region end up producing the largest antisymmetric scalae fluid pressure components, which in turn initiate the maximum BM velocity.

SUPPORTING MATERIAL

Seven figures, supporting data, and references (27–30) are available at http://www.biophysj.org/biophysj/supplemental/S0006-3495(14)00472-X.

The authors thank Kevin N. O'Connor for several critical readings of this paper, leading to numerous improvements.

This work was supported by R01 grants DC07910 and DC05960 from the National Institute on Deafness and Other Communication Disorders (NIDCD) of the National Institutes of Health (NIH), by Small Business Technology Transfer (STTR) funding (FA9550-07-C-0088) from the Air Force Office of Scientific Research (AFOSR), and by Naval Air Systems Command (NAVAIR) Small Business Innovation Research (SBIR) funding (N68335-10-C-0430).

REFERENCES

1. Viergever, M. A. 1978. Basilar membrane motion in a spiral-shaped cochlea. *J. Acoust. Soc. Am.* 64:1048–1053.

2. Steele, C. R., and J. G. Zais. 1985. Effect of coiling in a cochlear model. *J. Acoust. Soc. Am.* 77:1849–1852.

3. Cai, H., D. Manoussaki, and R. Chadwick. 2005. Effects of coiling on the micromechanics of the mammalian cochlea. *J. R. Soc. Interface.* 2:341–348.
4. Manoussaki, D., E. K. Dimitriadis, and R. S. Chadwick. 2006. Cochlea's graded curvature effect on low frequency waves. *Phys. Rev. Lett.* 96:088701.
5. Manoussaki, D., R. S. Chadwick, …, J. T. O'Malley. 2008. The influence of cochlear shape on low-frequency hearing. *Proc. Natl. Acad. Sci. USA.* 105:6162–6166.
6. Steele, C. R., N. Kim, and S. Puria. 2009. Hook region represented in a cochlear model. *In* Concepts and Challenges in the Biophysics of Hearing. N. P. Cooper and D. T. Kemp, editors. World Scientific, Singapore, pp. 323–329.
7. Stenfelt, S. 2011. Acoustic and physiologic aspects of bone conduction hearing. *Adv. Otorhinolaryngol.* 71:10–21.
8. Bárány, E. 1938. A contribution to the physiology of bone conduction. *Acta Otolaryngol.* 26 (*Suppl.*):1–223.
9. Békésy, G. 1949. The structure of the middle ear and the hearing of one's own voice by bone conduction. *J. Acoust. Soc. Am.* 21:227–241.
10. Kim, N., K. Homma, and S. Puria. 2011. Inertial bone conduction: symmetric and anti-symmetric components. *J. Assoc. Res. Otolaryngol.* 12:261–279.
11. Zhang, X., and R. Z. Gan. 2011. A comprehensive model of human ear for analysis of implantable hearing devices. *IEEE Trans. Biomed. Eng.* 58:3024–3027.
12. Homma, K., Y. Shimizu, …, S. Puria. 2010. Effects of ear-canal pressurization on middle-ear bone- and air-conduction responses. *Hear. Res.* 263:204–215.
13. Kim, N., C. R. Steele, and S. Puria. 2013. Superior-semicircular-canal dehiscence: effects of location, shape, and size on sound conduction. *Hear. Res.* 301:72–84.
14. Greenwood, D. D. 1990. A cochlear frequency-position function for several species—29 years later. *J. Acoust. Soc. Am.* 87:2592–2605.
15. Puria, S., W. T. Peake, and J. J. Rosowski. 1997. Sound-pressure measurements in the cochlear vestibule of human-cadaver ears. *J. Acoust. Soc. Am.* 101:2754–2770.
16. Aibara, R., J. T. Welsh, …, R. L. Goode. 2001. Human middle-ear sound transfer function and cochlear input impedance. *Hear. Res.* 152:100–109.
17. Gan, R. Z., B. P. Reeves, and X. Wang. 2007. Modeling of sound transmission from ear canal to cochlea. *Ann. Biomed. Eng.* 35:2180–2195.
18. Nakajima, H. H., W. Dong, …, J. J. Rosowski. 2009. Differential intracochlear sound pressure measurements in normal human temporal bones. *J. Assoc. Res. Otolaryngol.* 10:23–36.
19. Ren, T. 2005. The cochlear amplifier and Ca2+ current-driven active stereocilia motion. *Nat. Neurosci.* 8:132–134.
20. Shera, C. A. 2007. Laser amplification with a twist: traveling-wave propagation and gain functions from throughout the cochlea. *J. Acoust. Soc. Am.* 122:2738–2758.
21. Liu, Y. W., and S. T. Neely. 2010. Distortion product emissions from a cochlear model with nonlinear mechanoelectrical transduction in outer hair cells. *J. Acoust. Soc. Am.* 127:2420–2432.
22. Yoon, Y. J., S. Puria, and C. R. Steele. 2011. Feed-forward and feedbackward amplification model from cochlear cytoarchitecture: an interspecies comparison. *Biophys. J.* 100:1–10.
23. Tonndorf, J. 1962. Compressional bone conduction in cochlear models. *J. Acoust. Soc. Am.* 34:1127–1131.
24. Stenfelt, S., N. Hato, and R. L. Goode. 2002. Factors contributing to bone conduction: the middle ear. *J. Acoust. Soc. Am.* 111:947–959.
25. Carhart, R. 1950. Clinical application of bone conduction audiometry. *Arch. Otolaryngol.* 51:798–808.
26. Homma, K., Y. Du, …, S. Puria. 2009. Ossicular resonance modes of the human middle ear for bone and air conduction. *J. Acoust. Soc. Am.* 125:968–979.
27. Merchant, S. N., M. E. Ravicz, and J. J. Rosowski. 1996. Acoustic input impedance of the stapes and cochlea in human temporal bones. *Hear. Res.* 97:30–45.
28. Gundersen, T., O. Skarstein, and T. Sikkeland. 1978. A study of the vibration of the basilar membrane in human temporal bone preparations by the use of the Mössbauer effect. *Acta Otolaryngol.* 86:225–232.
29. Stenfelt, S., S. Puria, …, R. L. Goode. 2003. Basilar membrane and osseous spiral lamina motion in human cadavers with air and bone conduction stimuli. *Hear. Res.* 181:131–143.
30. Peterson, L. P., and B. P. Bogart. 1950. A dynamical theory of the cochlea. *J. Acoust. Soc. Am.* 22:369–380.

The importance of the hook region of the cochlea for bone-conduction hearing

Namkeun Kim[†], Charles R. Steele[†], and Sunil Puria[†,‡],

[†]*Department of Mechanical Engineering, Stanford University, Stanford, California 94305, USA*

[‡]*Department of Otolaryngology-Head and Neck Surgery, Stanford University, Stanford, California 94305, USA*

SUPPORTING MATERIAL

In this Supporting Material section, the model responses (e.g., the middle-ear pressure-gain function, cochlear impedance, basilar-membrane velocity, and best-frequency map) are compared with published data in order to provide validation for the current finite-element (FE) model. In addition, cochlear responses to air-conducted (AC) and bone-conducted (BC) excitations were calculated, and also compared with those of the previous FE model.

Validation of the FE model

The model-validation procedures are similar to those used in a previous study with a box model (1), with similar results in terms of the middle-ear (ME) pressure-gain function, cochlear input impedance, basilar-membrane (BM) velocity at specific locations, and cochlear best-frequency (BF) map.

Middle-ear pressure-gain function

In Figure S1, the ME pressure-gain function from the FE model, expressed as the ratio of the scalae-fluid pressure near the oval window (OW) to the acoustic pressure in the ear canal at the tympanic membrane (TM), P_{OW}/P_{EC}, is shown and compared with results from the literature (2–5). The FE results were consistent with experimental data to within about 5 dB from 0.3 kHz to 10 kHz.

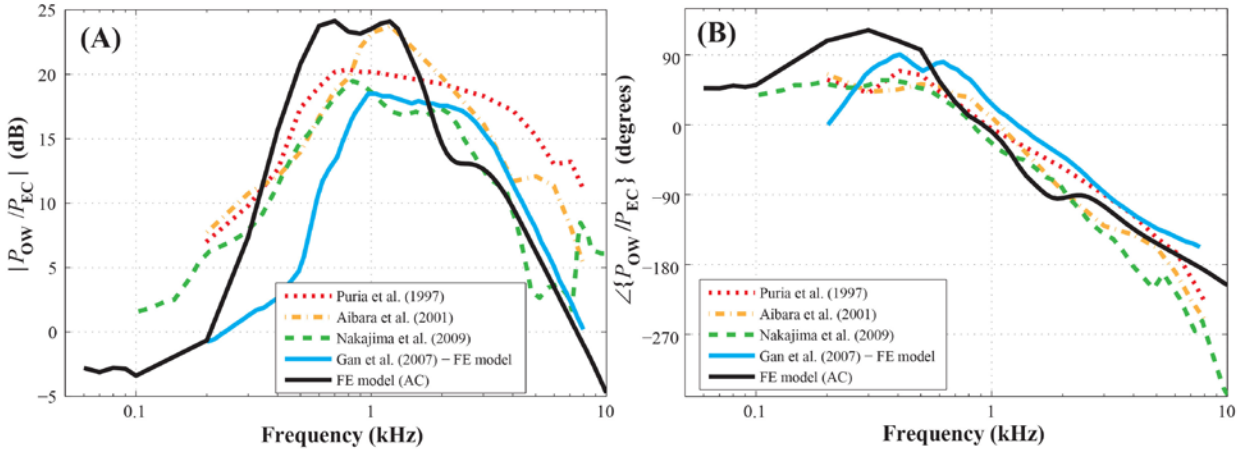

FIGURE S1. (A and B) The oval-window pressure, P_{OW}, to the ear-canal pressure, P_{EC}, middle-ear gain (P_{OW}/P_{EC}), for air-conducted (AC) excitation. (A) Magnitude in dB and (B) phase in degrees.

Cochlear input impedance

In Figure S2, the cochlear input impedance (Z_C) from the present model is shown alongside previous measured (3–6) and calculated (2) results. At frequencies below 0.5 kHz, the magnitude of Z_C for the current FE model falls within the range of the experimental data, but for higher frequencies it mostly remains somewhat above the comparison data in spite of their wide variance.

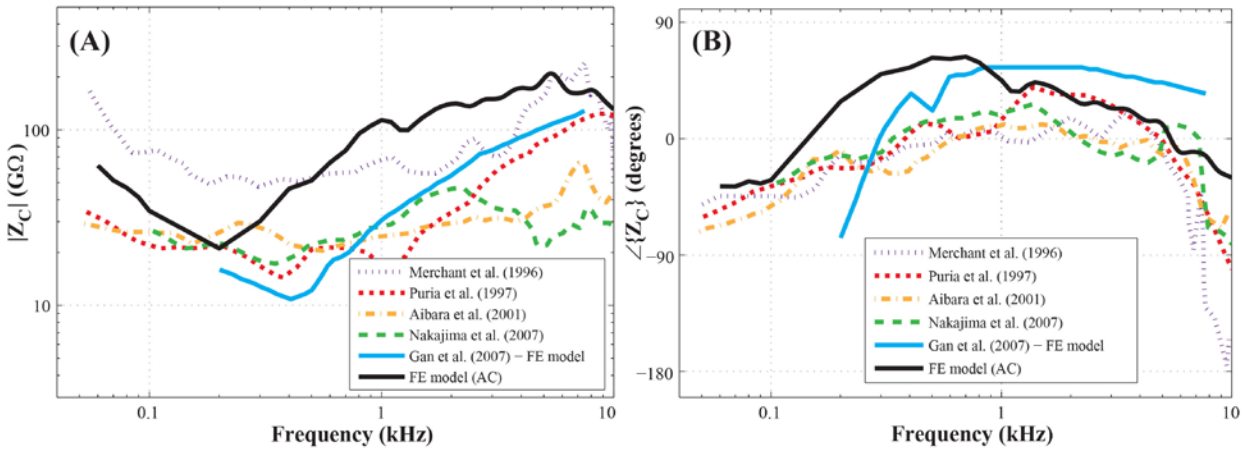

FIGURE S2. (A and B) Cochlear input impedance, Z_C, which is equal to P_{OW}/U_{OW}. (A) Magnitude in GΩ and (B) phase in degrees.

BM velocities at a specific location (χ = 12 mm)

The responses of V_{BM}, the velocity normal to the BM surface, to AC stimuli; and the relative BM velocity, ΔV_{BM}, to BC stimuli (where ΔV_{BM} is equal to V_{BM} minus the velocity of the bone, V_B), were measured at a specific BM location (approximately 12 *mm* from the base), and are shown in Figure S3. V_{BM} was normalized by the OW (i.e., stapes-footplate) velocity, V_{OW}, for AC stimuli. ΔV_{BM} was normalized by V_B for BC stimuli, and then $20\times log_{10}(\Delta V_{BM}/ V_B)$ was computed to represent '$\Delta V_{BM}/ V_B$' on a dB scale. For the model's AC results (Figure S3A), V_{BM}/V_{OW} reaches a maximum amplitude of 27 dB, between 4 and 5 kHz, which is reasonably consistent with the experimental data (7–8). For the model's BC results (Figure S3B), $\Delta V_{BM}/V_B$ reaches 21 dB for the maximum amplitude, at around 4 kHz, while the data from Stenfelt et al. (8) rises to 18 dB for the maximum amplitude, at around 2 kHz.

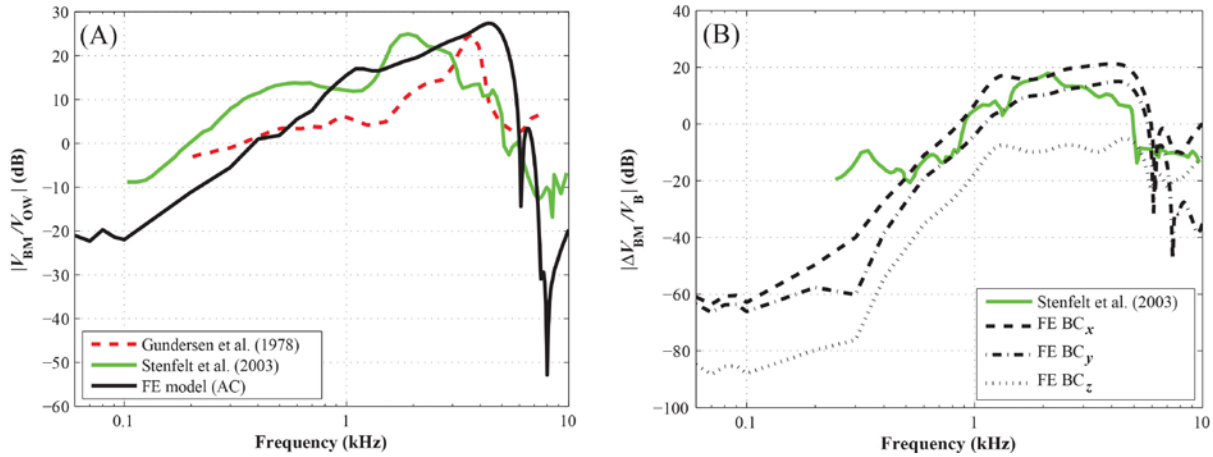

FIGURE S3. (A) The basilar-membrane (BM) velocity normalized by the stapes-footplate velocity, V_{BM}/V_{OW}, for AC excitation, and (B) the relative BM velocity ($\Delta V_{BM} = V_{BM} - V_B$) normalized by the BC bone-velocity input, $\Delta V_{BM}/V_B$, given for inputs in the direction of each of the three orthogonal axes, *x*, *y*, and *z* (*i.e.*, lateral, superior, and medial directions of the skull, respectively). The BM velocity for both modeled and experimental responses was calculated at χ = 12 *mm* from the RW.

Cochlear best-frequency map

The FE-simulated best-frequency (BF) cochlear map is shown in Figure S4, and is compared with the cochlear map estimated from an equation found in (9). The BF map from the FE model is in good agreement with the data except for the BFs below 200 Hz, which correspond to BM locations greater than χ = 30 *mm*. This agreement between the simulated and measured BF maps was achieved by iteratively tuning the elastic modulus values of the BM for AC excitation. It should be noted that the model's BF map is a serrated line rather than a smooth line like Greenwood's results for the following reason: in local regions where the curvature of the coiled BM is large, the width of the BM in the model does not increase smoothly along the length of the BM from base to apex, and as a result, the location of the node where the BM velocity is calculated ends up straying slightly from the centerline of the BM in these regions.

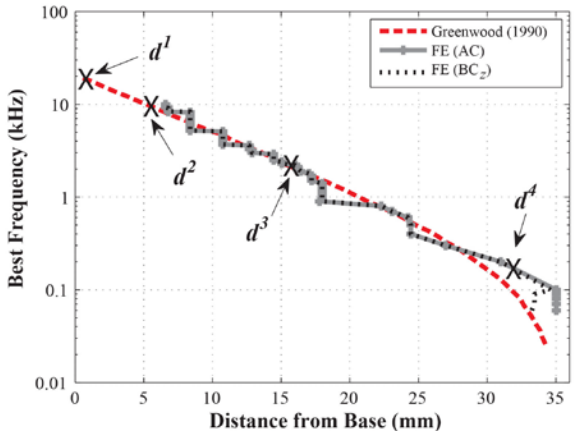

FIGURE S4. Simulated best-frequency (BF) maps for AC excitation and BC excitation given in the *z* direction, along with results from Greenwood (9). The results in the *x* and *y* directions were almost identical to the one shown for the *z*-directional excitation. 'X' marks on the BF plot indicate the four different BM locations (0.8, 5.8, 15.63, and 33.06 *mm*) for which the d^1, d^2, d^3, and d^4 directions are respectively defined.

Cochlear responses to AC and BC excitation

Having thus validated the FE model, the next step was to simulate and analyze the symmetric (fast-wave) and anti-symmetric (slow-wave) response characteristics of the scalae-fluid pressure and volume velocities of the OW and round window (RW) due to AC and BC excitations. Normalized BM-velocities are plotted along the length of the BM in Figures S5, S6, and S7, for particular input frequencies.

BM-velocity responses to AC and BC excitation

Figure S5 shows the simulated relative BM-velocity distribution along the length of the BM, $\Delta V_{\mathrm{BM}}(\chi)$, in response to BC excitations of the rigid bone forming the boundaries of the model. The results are shown for three frequencies: 0.5, 1, and 7 kHz. The BC cases are normalized with respect to the velocity magnitude of the rigid bone, V_{B}. Figure S5 also shows the BM-velocity distribution in response to AC excitation, $V_{\mathrm{BM}}(\chi)$, normalized by the corresponding stapes velocity, V_{OW}. The overall shape of the BM-velocity distribution magnitude for each respective frequency is similar among the different excitation cases, including between the AC- and BC-excitation cases. However, the primary difference among the three input-frequency cases (0.5, 1.0, and 7.0 kHz) is that their magnitudes are shifted with respect to one another. The phase responses for the different input frequencies are similarly shifted with respect to one another.

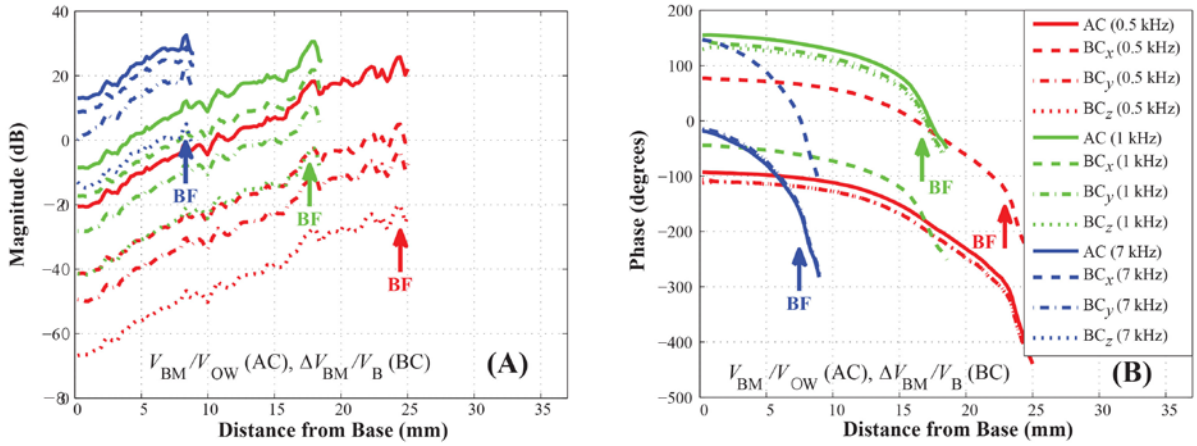

FIGURE S5. Magnitude (A) and Phase (B) of BM-velocity profiles along the length of the BM, $V_{BM}(\chi)$, normalized by the stapes velocity, V_{OW}, for AC excitation (solid lines); and the relative BM-velocity profile, $\Delta V_{BM}(\chi)$, normalized by the magnitude of the base bone velocity, V_B, for BC excitations. Excitation frequencies of 0.5, 1, and 7 kHz were used. The BC curves indicate the sensitivity of the cochlea to BC excitations in the *x* (dashed lines), *y* (dash-dotted lines), and *z* (dotted lines) directions. The legend applies to both (A) and (B), and the arrows labeled "BF" indicate the best-frequency locations on the BM corresponding to each stimulus frequency.

Normalization of the BM velocity by anti-symmetric and symmetric volume-velocity components

Figure S6 shows, for the present coiled-cochlea model, the BM-velocity (V_{BM}) and relative BM-velocity (ΔV_{BM}, where ΔV_{BM} is defined as '$V_{BM} - V_B$', with V_B being the BC velocity used to stimulate the model) distributions in response to AC and BC excitations, respectively. These quantities are normalized by both the anti-symmetric, U_A, and symmetric, U_S, volume-velocity components (in Figures S6A and S6B, respectively). The results are shown for 0.5, 1, and 7 kHz. As can be seen in Figure S6(A), the results for the different excitation cases show better alignment with each other when they are normalized by the anti-symmetric volume-velocity component, U_A (as compared to Figure S5A, in which the results are normalized by the stapes velocity and bone velocity for AC and BC, respectively). In the case of the 7 kHz results, the magnitudes of the normalized BM velocities (V_{BM}/U_A for AC and $\Delta V_{BM}/U_A$ for BC) show at most a 2–5 dB difference between one another, whereas for the other frequencies, 0.5 and 1 kHz, the corresponding normalized BM velocities for AC and BC stimuli overlap with one another such that they appear to form single lines. In contrast, when normalized by the symmetric volume-velocity component, U_S (Figure S6B), the results for a given frequency reveal misalignments between the different excitation methods. This demonstrates that the anti-symmetric volume-velocity component, U_A, correlates with the BM vibration better than the symmetric volume-velocity component, U_S. This was also the finding for the simplified box model (1).

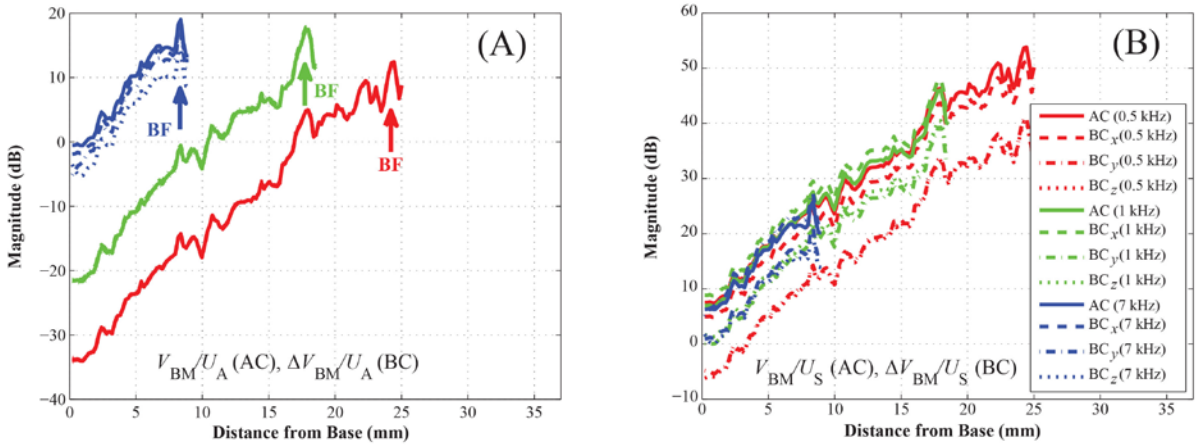

FIGURE S6. (A and B) BM velocity distributions along the length of the BM, $V_{BM}(\chi)$ and $\Delta V_{BM}(\chi)$ (defined as '$V_{BM} - V_B$', where V_B is the BC velocity used to stimulate the model), in response to AC and BC excitations, respectively, at 0.5, 1, and 7 kHz. The results are normalized by (A) the anti-symmetric volume-velocity (slow-wave) component, U_A, and (B) the symmetric volume-velocity (fast-wave) component, U_S.

Decomposition of the cochlear-fluid pressure into symmetric and anti-symmetric components

Figure S7 shows the anti-symmetric and symmetric pressure components, $P_A(\chi)$ and $P_S(\chi)$, normalized by U_A, at 1 and 7 kHz. In the figure, the magnitudes of $P_A(\chi)$ for different excitation cases become aligned with one another up to the corresponding BF position when normalized by U_A, whereas this is not the case for $P_S(\chi)/U_A$. This result follows a similar pattern to the normalized BM velocities ($V_{BM}(\chi)/U_A$ for AC and $\Delta V_{BM}(\chi)/U_A$ for BC), as shown in Figure S6(A), in that the anti-symmetric normalized velocity and pressure profiles ($V_{BM}(\chi)/U_A$, $\Delta V_{BM}(\chi)/U_A$, and $P_A(\chi)/U_A$) all feature overlapping lines for their different excitation cases.

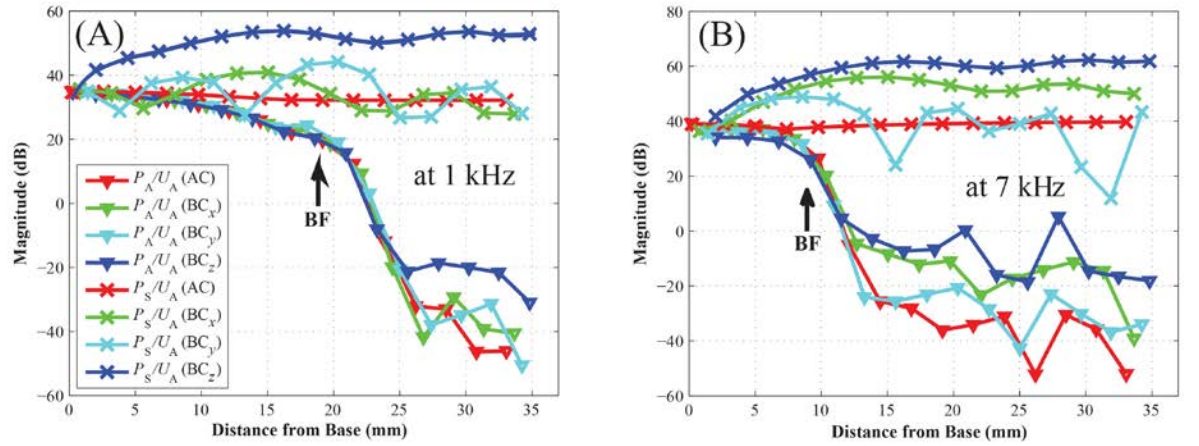

FIGURE S7. (A and B) Cochlear scalae-fluid pressure distributions along the BM length (*i.e.*, the anti-symmetric pressure, $P_A(\chi)$, and symmetric pressure, $P_S(\chi)$), in response to AC and BC excitations, normalized by the corresponding anti-symmetric volume-velocity component, U_A, at (A) 1 kHz and (B) 7 kHz.

Comparisons with the simplified box model

Based on a simplified box cochlear model, the BM was shown to primarily respond to the anti-symmetric excitation components (*i.e.*, the slow traveling wave; 10) generated at the OW and RW, regardless of whether the components were produced via AC or BC excitation (1). In this study, the relationships between the anti-symmetric pressure and volume-velocity components were investigated using a more anatomically realistic coiled cochlear model. As shown in Figure S6, regardless of the excitation type, the BM-velocity response was correlated with the anti-symmetric rather than the symmetric volume velocity. In addition, Figure S7 shows that the anti-symmetric volume velocity was closely related to the anti-symmetric pressure along the BM length. In short, regardless of the excitation type or direction, the anti-symmetric scalae-fluid pressure and anti-symmetric volume velocity are both highly correlated with the BM velocity. These results from the coiled model are consistent with those from the simplified box model.

SUPPORTING MATERIAL REFERENCES

1. Kim, N., K. Homma, and S. Puria. 2011. Inertial bone conduction: Symmetric and anti-symmetric components. *J. ARO.* 12:261-279.
2. Gan, R.Z., B.P. Reeves, and X. Wang. 2007. Modeling of Sound Transmission from Ear Canal to Cochlea. *Ann. Biomed. Eng.* 32: 847-859.
3. Puria, S., W.T. Peake, and J.J. Rosowski. 1997. Sound-pressure measurements in the cochlea vestibule of human cadaver ears. *J. Acoust. Soc. Am.* 101:2754-2770.
4. Aibara, R., J.T. Welsh, S. Puria, and R.L. Goode. 2001. Human middle-ear sound transfer function and cochlear input impedance. *Hear. Res.* 152:100-109.
5. Nakajima, H.H., W. Dong, E.S. Olson, S.N. Merchant, M.E. Ravicz, and J.J. Rosowski. 2009. Differential intracochlear sound pressure measurements in normal human temporal bones. *J. ARO.* 10:23-36.
6. Merchant, S.N., M.E. Ravicz, and J.J. Rosowski. 1996. Acoustic input impedance of the stapes and cochlea in human temporal bones. *Hear. Res.* 97:30-45.
7. Gundersen, T., Φ. Skarstein, and T. Sikkeland. 1978. A study of the vibration of the basilar membrane in human temporal bone preparations by the use of the Mössbauer effect. *Acta Otolaryngol.* 86:225-232.
8. Stenfelt, S., S. Puria, N. Hato, and R.L. Goode. 2003. Basilar membrane and osseous spiral lamina motion in human cadavers with air and bone conduction stimuli. *Hear. Res.* 181:131-143.
9. Greenwood, D.D. 1990. A cochlear frequency-position function for several species-29 years later. *J. Acoust. Soc. Am.* 87:2592-2605.
10. Peterson, L.P., and B.P. Bogart. 1950. A dynamical theory of the cochlea. *J. Acoust. Soc. Am.* 22:369-380.